GEOFIZIKA VOL. 42 2025

*DOI: 10.15233/gfz.2025.42.6*
*Original scientific paper*

# Characteristics of the 2025 Santorini-Amorgos seismic swarm

*Emil Oynakov, Irena Aleksandrova* and Mariya Popova*

National Institute of Geophysics, Geodesy and Geography, Bulgarian Academy of Sciences, Sofia, Bulgaria

*Received 8 April 2025, in final form 22 June 2025*

This study investigates the spatiotemporal evolution and scaling characteristics of the 2025 seismic swarm in the Santorini-Amorgos region, one of the most seismically and volcanically active zones in the Aegean arc. Using a high-resolution earthquake catalog including 1,601 events ($M_L \geq 2.9$), we analyze variations in key statistical parameters – including b-value, fractal dimension (*Dc*), scaling exponent (*ab*), and the q-parameter – within cumulative time windows. Our findings reveal a marked decrease in b-value and simultaneous increase in *Dc* during the swarm's activation phase, consistent with an inverse energy cascade and progressive rupture. The spatial extent of the seismic swarm (*L*) contracts significantly before expanding during the decay phase, and vertical migration of the seismic barycenter suggests a fluid-triggered nucleation process. 3D visualizations confirm fault-aligned clustering and upward migration patterns, supporting a hybrid rupture mechanism governed by both tectonic faulting and fluid diffusion. These results provide critical insights into the complex dynamics of swarms in extensional volcanic environments and highlight the relevance of fractal and scaling analysis for short-term seismic hazard assessment.

*Keywords*: seismic swarm, Santorini-Amorgos, b-value, fractal dimension, rupture scaling; fluid–fault interaction, earthquake migration

## 1. Introduction

Laboratory studies of transient processes in seismicity allow for the identification of characteristic changes in statistical parameters of the seismic regime (Scholz, 2019). Experimental results reveal temporal changes in the slope of the recurrence plot (*b*-value) during earthquake seismic swarms. During the activation phase, the *b*-value tends to decrease, while it increases during the decay

phase. The effect-minimum *b*-value coinciding with peak seismic activity-becomes more pronounced under higher stress levels (Mitchell and Faulkner, 2008).

Similar *b*-value (slope of the Gutenberg-Richter relationship) (Gutenberg and Richter, 1944) variations have been observed in experiments where microseismicity is induced through pressurized water injection (Keranen, and Weingarten, 2018). These findings support the idea that the rupture process changes over time, with larger events becoming more dominant during activation, and smaller ones during decay-reflecting a dynamic evolution of seismic energy release. A decrease in the *b*-value during the activation stage suggests that the share of stronger events increases over time-indicating a transition from micro- to macro-fracturing. Conversely, in the decay phase, smaller events dominate, representing a reverse energy cascade.

This process reflects the fractal organization of seismicity: as rupture scales shift dynamically, they reveal evolving structural heterogeneity. Notably, a decrease in the *b*-value and a persistent $a_b < 1$ have been associated with the presence of overpressurized fluids, which reduce effective normal stress and promote the occurrence of larger events (Mogi, 1963; Wyss, 1973). These trends suggest that fluid–fault interactions may have played a central role in modulating rupture behavior during the swarm.

## 2. Seismicity of the Santorini-Amorgos region

The Santorini-Amorgos region, located in the central Aegean Sea, is one of the most seismically and volcanically active zones in the eastern Mediterranean. The high seismic activity observed in this area results from the convergence of the Aegean portion of the Eurasian lithospheric plate with the African plate – an interaction zone commonly referred to as the Hellenic Benioff Zone (Papazachos and Papazachou, 1997). This subduction interface is among the most seismically active in Europe, accommodating substantial tectonic deformation.

Greece has a long-documented history of destructive seismic events, recorded in antiquity by authors such as Cicero, Strabo, and Pliny. According to Cicero, one of the earliest known historical records describes a powerful earthquake in 550 BCE that destroyed the city of Sparta and triggered the collapse of part of Mount Taygetus (Ambraseys, 2009). The island of Santorini has experienced numerous major earthquakes and volcanic eruptions throughout history prior to 1900 (Ambraseys, 2009). The most notable of these was the Minoan eruption, which occurred about 3,600 years ago during the Late Bronze Age. This event is believed to have wiped out the island's thriving settlements and ecosystems. Estimated to have ejected about 30 $km^3$ of magma in the form of pumice and volcanic ash, the eruption buried the island, its inhabitants, and its material culture under a thick pyroclastic layer. More recent volcanic activity occurred in

1939, 1941, and 1950 (Arriaga et al., 2008), coinciding with increased geothermal and moderate seismic activity in the caldera.

The largest earthquake to strike Greece in the 20th century occurred on July 9, 1956. With an epicenter near the island of Amorgos, this event had a moment magnitude of 7.8 as estimated by B. Gutenberg in Pasadena and reported by the International Seismological Summary (ISS). The earthquake resulted in 53 fatalities and caused widespread destruction, especially on the island of Santorini. Additionally, it generated a local tsunami that affected the coastlines of the Cyclades, Dodecanese, Crete, and western Anatolia (Okal et al., 2009).

## 3. Data and methodology

This study analyzes the seismic swarm that occurred in the Santorini--Amorgos region in February and March 2025. The Santorini-Amorgos region lies within an extensional tectonic regime associated with the Hellenic volcanic arc. The Santorini-Amorgos region lies within an extensional tectonic regime associated with the Hellenic volcanic arc. The area hosts a complex system of active normal and oblique faults, predominantly trending NE–SW and N–S, which accommodate crustal thinning and caldera-related deformation. These include the well-documented Amorgos Fault and subsidiary structures within the Santorini caldera system (Nomikou et al., 2012; Andinisari et al., 2021; Bohnhoff et al., 2006). The main active faults depicted in Fig. 1 were compiled from published seismotectonic maps, bathymetric surveys, and seismic reflection profiles available through the GReDaSS database and related studies. The main active faults (https://edsf13.ingv.it/sharedata/SHARE_WP3.2_Map.html) depicted in Fig. 1 were compiled from previously published seismotectonic maps and fault databases derived from high-resolution bathymetry (https://topex.ucsd.edu/) and seismic reflection profiles.The dataset consists of 3755 events with local magnitudes $M_L \geq 0.5$, recorded by the Hellenic Seismological Network (NOA) (Fig. 1).

All magnitudes in the dataset are reported as local magnitudes ($M_L$) according to the Hellenic Seismological Network (NOA). Prior to determining the magnitude of completeness (*Mc*), the dataset was checked for consistency in magnitude scale. *Mc* was then estimated as 2.9 using the maximum curvature method (Figs. 2 and 3). After filtering for quality and removing duplicates, 1,601 events remained suitable for advanced analysis. To assess temporal variations in magnitude distribution, we computed daily cumulative frequency-magnitude distributions. The overlapping colored curves in Fig. 2 represent the progressive build-up of events day by day from 01 February to 03 March 2025. This approach allows us to visually confirm the stability of $Mc = 2.9$ across the swarm's evolution.

The earthquake catalog used in this study does not explicitly include hypocenter location uncertainties. Therefore, we applied an indirect method to estimate

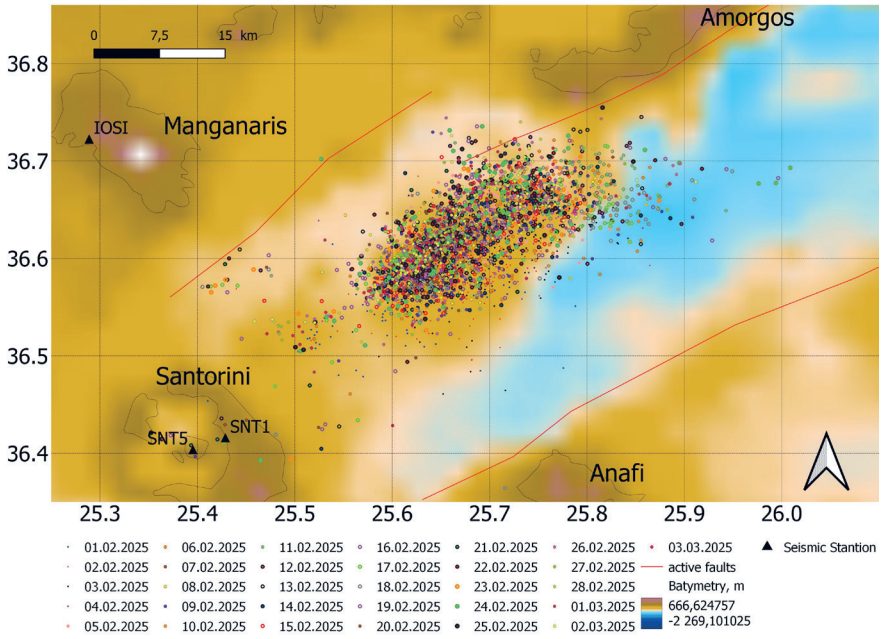


**Figure 1.** Epicentral distribution of the 2025 Santorini-Amorgos swarm colored by date. Active faults are shown in red.

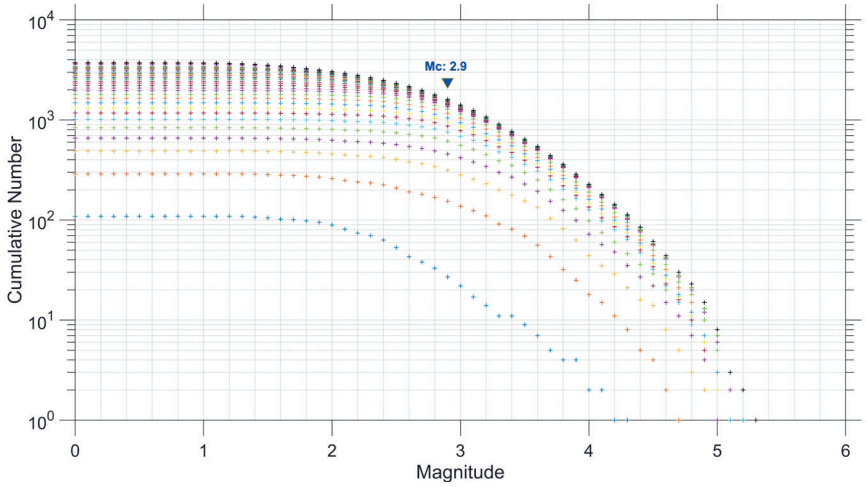


**Figure 2.** Cumulative frequency–magnitude distributions (FMDs) computed for individual days during the 2025 Santorini-Amorgos swarm (from 01 February (blue color) to 03 March). Each colored curve corresponds to one day, showing the progressive accumulation of events over time. The magnitude of completeness ($Mc = 2.9$) was determined using the maximum curvature method and is marked by the blue inverted triangle. The black curve represents the FMD for the entire dataset.

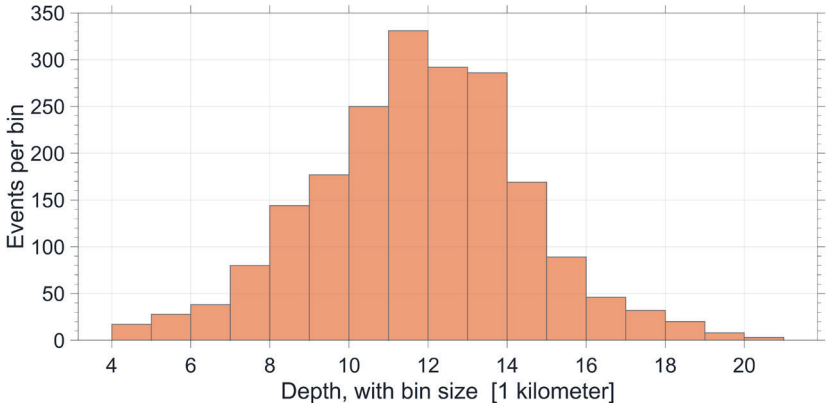


**Figure 3.** Histogram of event (magnitudes $M_L > 0.5$) depths showing a concentration of earthquakes between 10 and 14 km.

location error based on the lower bound of the scaling range in the fractal correlation integral (Mandelbrot, 2002; Grassberger and Procaccia, 1983). To assess the reliability of this approach, we manually retrieved hypocenter errors for a subset of events from the NOA database. The reported uncertainties (typically 2.5–4.0 km horizontally and 3–5 km vertically) are consistent with our estimated resolution of ~ 3.4 km, supporting the validity of the method.

In real-world data, linearity is observed only within a specific range of distances, referred to as the scaling range. According to (Mandelbrot, 2002), the boundaries of this range are known as the inner and outer thresholds. In the context of seismicity, the upper threshold is typically determined by the size of the earthquake cluster or the spatial extent of the catalog. Conversely, the lower threshold corresponds to the uncertainty in hypocenter locations.

By identifying the lower limit of the scaling range, one can infer the effective spatial resolution of earthquake location estimates. In this study, the correlation integral was employed to assess the fractal properties of seismicity. This integral serves as a statistical approximation of the distribution function of inter-event distances.

The lower of the fractal scaling range to estimate the spatial resolution limit – *i.e.*, the uncertainty in earthquake locations. This is a known method in fractal analysis (Wiemer and Wyss, 2000).

Figure 4 presents the correlation integral plots calculated for cumulative time windows, which quantify the spatial clustering of earthquakes in the catalog. The upper bound of the scaling range remains relatively stable across time and reflects the extent of the active seismic region (20–30 km). The lower bound, by contrast, is interpreted as the effective resolution limit – that is, the shortest distance at which clustering can be reliably distinguished, which in turn depends

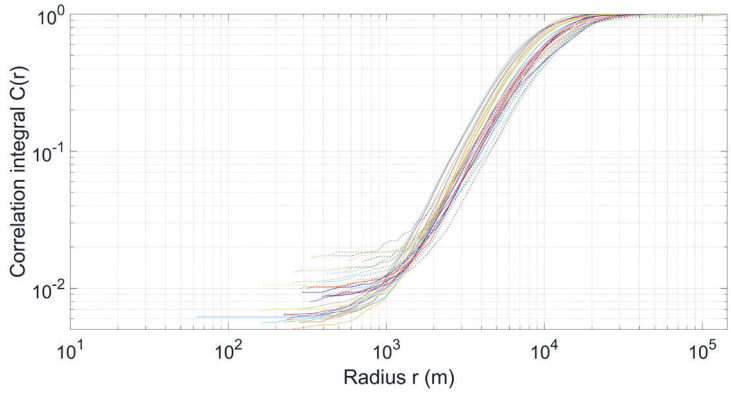


**Figure 4.** Correlation integral $C(r)$ in logarithmic scale representing fractal clustering patterns.

on location uncertainty. Following established approaches in fractal seismicity analysis (*e.g.*, Wiemer and Wyss, 2000), we use this threshold to estimate the average hypocenter location error. Figure 5 shows this lower bound, which corresponds to a spatial uncertainty of approximately 3.4 km.

To investigate the time-dependent behavior of the seismic swarm, we calculated several statistical and geometrical parameters using cumulative moving windows with one-day increments. The following methods and parameters this study used:

The $b$-value was calculated using the maximum likelihood method based on the Gutenberg-Richter law. A drop-in $b$-value typically indicates the emergence

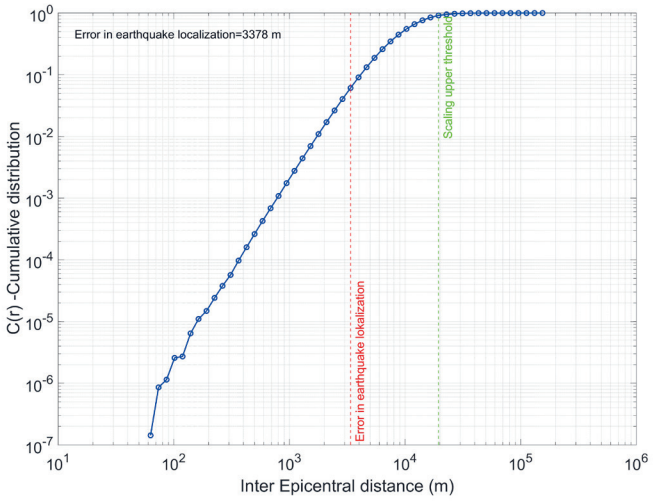


**Figure 5.** Spatial resolution and localization error (~3.400 m) relative to the correlation scale.

of stronger seismic events or more heterogeneous stress fields. Equation (1), which provides the maximum likelihood estimate of the *b*-value, follows the formulation introduced by Aki (1965) and Utsu (1965):

$$b = \frac{\log \mathrm{e}}{M_{mean} - M_{min}}, \quad \sigma_b = \frac{b}{\sqrt{N}} \tag{1}$$

where $\sigma_b$ is the standard deviation of the *b*-value, and $N$ is the number of events used in the calculation. $M_{mean}$ is the average magnitude of events above the completeness threshold $Mc$, and $M_{min}$ is the minimum magnitude considered ($Mc$). This equation derives the *b*-value from the Gutenberg-Richter law using the maximum probability estimation method.

Fractal dimension ($Dc$) was determined using the Grassberger-Procaccia method applied in 4D space (latitude, longitude, depth, and time), reflecting the degree of spatial-temporal clustering. This is the correlation integral used to estimate the fractal dimension ($Dc$), where $d_{ij}$ is the distance between earthquake pairs and $H$ is the Heaviside function:

$$C(r) = \frac{1}{N(N-1)} \sum_{i=1}^{N} \sum_{j=j+1}^{N} \theta(r - d_{ij}) \tag{2}$$

$C(r)$ – the correlation integral; it counts the number of event pairs that are separated by a distance less than $r$;

$H$ – the Heaviside step function, which equals 1 when $r > d_{ij}$, and 0 otherwise;

$d_{ij}$ – the Euclidean distance between seismic events $i$ and $j$;

$N$ – the total number of earthquakes in the catalog.

$$d_{ij} = \sqrt{\left(X_i - X_j\right)^2 + \left(Y_i - Y_j\right)^2 + \left(Z_i - Z_j\right)^2 + V_T^2 \left(T_i - T_j\right)^2} \tag{3}$$

$X_i$, $Y_i$, $Z_i$ are the spatial coordinates (longitude, latitude, depth) of event $ii$;

$T_i$ is the origin time of event $ii$;

$V_T$ is a scaling factor that converts temporal separation into an equivalent spatial scale (typically in km/day).

The last term accounts for the contribution of time differences to the overall spatiotemporal distance.

$$D_c = \lim_{r \to 0} \frac{d \log C(r)}{d \log r} . \tag{4}$$

The scaling exponent ($a_b$) and the nonextensivity parameter ($q$) were computed to quantify deviations from linear scaling between earthquake magnitude and spatial dispersion. A value of $a_b < 1$ indicates that larger-magnitude events dominate the rupture geometry, deviating from self-similar scaling. The $q$-parameter,

derived from nonextensive statistical mechanics, characterizes the degree of clustering: values of $q > 1$ suggest long-range correlations and non-Poissonian behavior. These metrics have been previously applied in seismology to identify complexity and hierarchical structure in fault networks (Telesca, 2010; Abe and Suzuki, 2003):

$$E \approx M^{\alpha_b} . \tag{5}$$

The $q$-parameter, derived from Tsallis nonextensive statistical mechanics, captures the degree of clustering and correlation in the seismic system. A value of $q = 1$ corresponds to the classical Boltzmann-Gibbs distribution, while $q > 1$ suggests long-range interactions or hierarchical fault structure. This metric has been used to characterize the complexity of earthquake sequences (Telesca, 2010; Abe and Suzuki, 2003).

$$q = \frac{D_C}{\alpha_b} - b . \tag{6}$$

Migration velocity $V_m$ is calculated as the ratio of maximum spatial distance ($d_{max}$) to the time duration of the swarm ($T_{max}$):

$$V_m = \frac{d_{max}}{T_{max} - T_{min}} . \tag{7}$$

The effective swarm size ($L$) is approximated as four times the radius of gyration ($R_g$):

$$L = 4R_g \tag{8}$$

This defines the radius of gyration ($R_g$), where ($x_0$, $y_0$, $z_0$) is the centroid of the swarm and ($x_0$, $y_0$, $z_0$) are the coordinates of each event. It is used to characterize the spatial extent of the swarm.

$$R_g = \sqrt{\frac{1}{N}\sum_{i=1}^{N}(x_i - x_0)^2 + (y_i - y_0)^2 + (z_i - z_0)^2} , \tag{9}$$

where $M'$ is the average magnitude of events above the completeness threshold $Mc$, and $M_{min}$ is the minimum magnitude considered ($Mc$). This equation derives the $b$-value from the Gutenberg-Richter law using the maximum likelihood estimation method. We define the overall swarm size $L = 4\,R_g$ as four times the radius of gyration, following previous studies (*e.g.*, Mogi, 1963; Wiemer and Wyss, 2000).

Brief explanations of the basic equations used:

Migration velocity $V_m$ is calculated as the ratio of maximum spatial distance ($d_{max}$) to the time duration of the swarm ($T_{max}$).

The effective swarm size ($L$) is approximated as four times the radius of gyration ($R_g$).

This defines the radius of gyration ($R_g$), where ($x_0$, $y_0$, $z_0$) is the centroid of the swarm and ($x_i$, $y_i$, $z_i$) are the coordinates of each event. It is used to characterize the spatial extent of the swarm.

Migration of the seismic swarm was assessed by tracking the barycenter (centroid) depth over time, along with the migration velocity ($V_m$), derived from the spatial extent divided by the duration.

## 4. Results

The time-dependent behavior of key seismic parameters—b-value, fractal dimension ($Dc$), scaling exponent ($a_b$), and $q$-parameter—was analyzed using cumulative time windows. A clear pattern emerges: $b$-value exhibits a distinct decrease during the early activation stage of the seismic swarm, while $Dc$ increases significantly, peaking approximately February 8 and 22, 2025 (Figs. 6 and 7). These dates coincide with observed clustering and spatial compression of events.

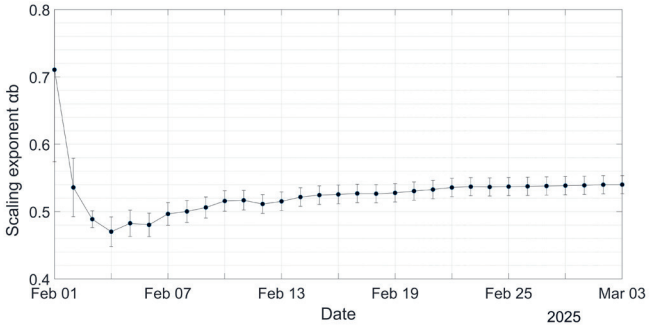


**Figure 6.** Temporal evolution of the cumulative b-value, calculated using all events from February 1 to each corresponding day. Error bars represent the standard deviation based on the maximum likelihood estimation.

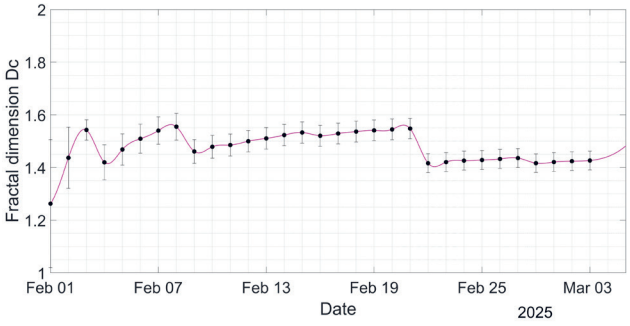


**Figure 7.** Fractal dimension Dc computed daily, indicating variation in spatial clustering.

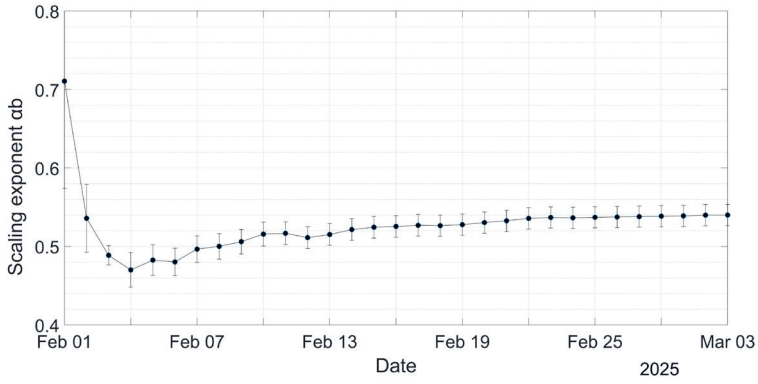


**Figure 8.** Temporal trend of the scaling exponent αb across the seismic sequence.

The calculated scaling exponent αb remains below 1 throughout most of the seismic swarm, indicating a dominance of higher-magnitude events and a deviation from simple self-similar scaling. This pattern is commonly associated with increasing stress heterogeneity or elevated stress levels. Simultaneously, the q-parameter starts above 2.0 and gradually declines, suggesting a shift from a fluid-dominated to a fault-controlled regime. Together, these trends point to a progressive localization of stress and rupture along pre-existing fault planes (Figs. 8 and 9).

The temporal variation of $L$ (Fig. 10) reveals significant spatial contraction during the activation phase, reaching a minimum value of approximately 28.7 km on February 8, 2025, which coincides with the maximum of the fractal dimension $Dc$. This contraction likely reflects a spatial focusing of seismic energy along activated fault segments. Following the peak, $L$ gradually increases again, indicating a dispersal of seismicity during the decay phase.

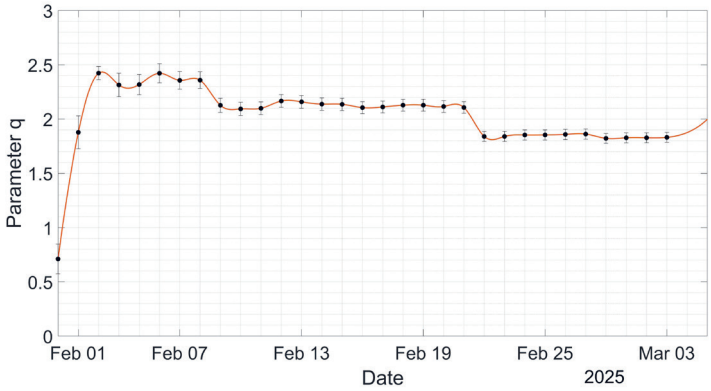


**Figure 9.** $q$-parameter indicating the level of clustering in the seismic catalog over time.

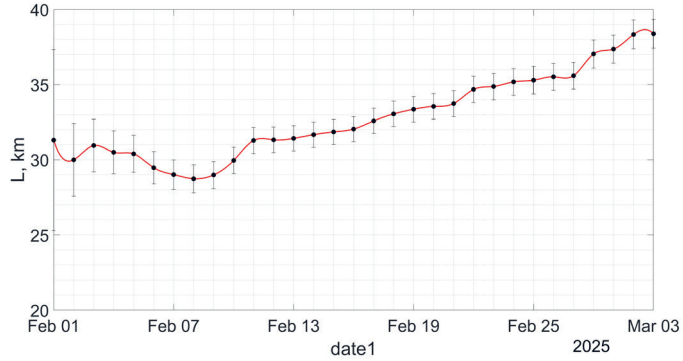


**Figure 10.** Temporal change of swarm spatial extent ($L$) derived from the radius of gyration.

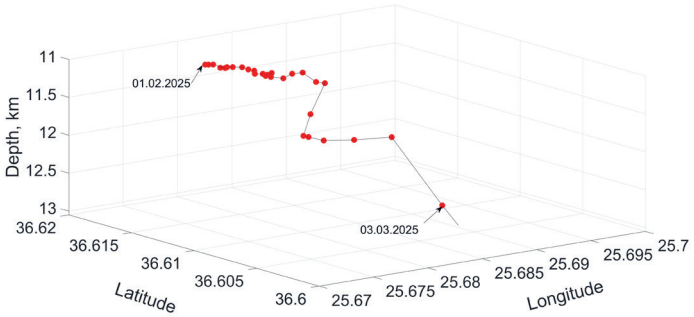


**Figure 11.** 3D migration of the barycenter of the swarm with increasing shallowness.

The spatial evolution of the swarm was quantified using the parameter $L$, representing the effective diameter of the seismic cluster. It is calculated from the radius of gyration ($R_g$) as $L = 4 \times R_g$. The temporal variation of $L$ (Fig. 10) reveals a notable spatial contraction during the activation phase, reaching a minimum of approximately 28.7 km around February 8, 2025, coinciding with the peak in fractal dimension $Dc$. This suggests spatial focusing of seismic activity along activated fault segments. Following this peak, $L$ gradually increases, indicating a dispersal of seismicity during the decay phase.

The barycenter of seismicity reveals a vertical migration from 11.3 km to 12.6 km depth over the course of the seismic swarm (Fig. 11). This vertical migration pattern may be indicative of a hybrid rupture mechanism, where upward fluid movement along permeable fault zones contributes to the nucleation process. While this interpretation aligns with fluid-driven models proposed in other volcanic swarms, it remains a working hypothesis pending direct geophysical or geochemical confirmation.

To enhance the spatial understanding of rupture propagation, a set of 3D visualizations was produced (figs 11–13). These provide a structural view of swarm migration and organization:

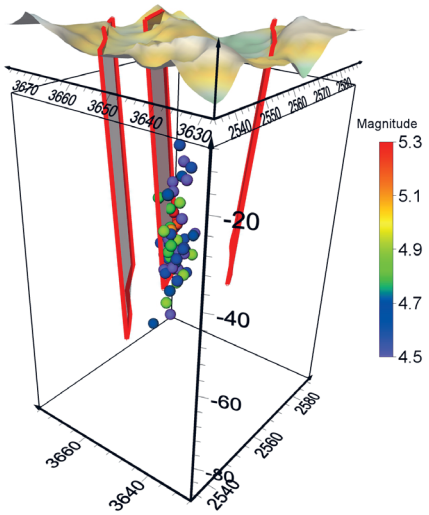


**Figure 12.** 3D spatial distribution of $M \geq 4.5$ earthquakes with vertical fault segments shown in red.

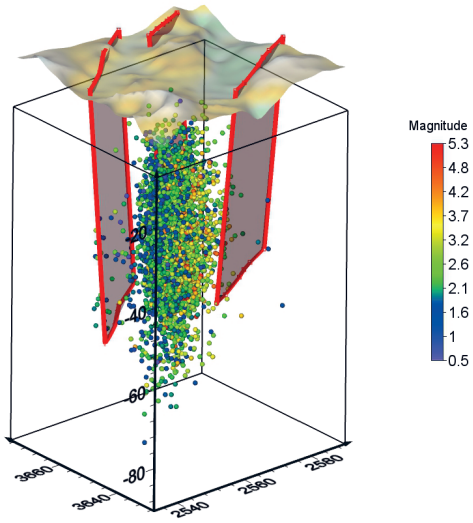


**Fig**. 13. Full 3D visualization of the seismic swarm with active fault planes and magnitude color scale.

• Figure 11 illustrates the 3D upward migration of the barycenter from approximately 13.05 km to 9.6 km depth, indicative of pressure-driven rupture or fluid migration through a vertical conduit.

• Figure 12 displays the distribution of events with $M \geq 4.5$, concentrated in a narrow vertical volume suggestive of activation of a steep fault zone.

• Figure 13 shows the complete 3D distribution of seismicity, aligned predominantly along NE–SW trending structures. This is consistent with the regional extensional tectonics of the Santorini-Amorgos rift system.

Together, these results support the interpretation of a dynamically evolving seismic swarm influenced by both fault geometry and fluid participation.

To complement the statistical evaluation, the spatiotemporal evolution of seismicity was visualized in 3D plots (figs 12–13). These reveal several important structural characteristics of the swarm:

Figure 12 illustrates the location of higher-magnitude earthquakes ($M \geq 4.5$) concentrated in a narrow vertical volume, suggesting activation of a single steep fault or fault zone.

Figure 13 presents the full 3D distribution of the swarm, showing a clear alignment along NE–SW striking structures, consistent with the known tectonic regime of the Santorini-Amorgos rift system.

Together, the results from $L(t)$ analysis and 3D visualization provide evidence of a dynamically evolving rupture environment influenced by both structural geometry and possible fluid involvement.

## 5. Discussion

The Santorini-Amorgos region is characterized by high thermal gradients and a complex heterogeneous crust, typical of extensional volcanic systems (Warren and Latham, 1970; Mogi, 1963). Previous studies (*e.g.*, McNutt, 2025) have shown that a decrease in b-value during volcanic swarms may reflect increased magmatic pressure, potentially indicating elevated eruption risk. Our observations of decreasing $b$ and increasing $Dc$ are thus consistent with such behavior and may offer critical early warning indicators.

The decrease in b-value combined with the increase in $Dc$ during the seismic swarm's peak activity supports the concept of an inverse energy cascade – a process where small-scale ruptures propagate and coalesce into larger ones. This is indicative of increasing fault complexity and stress concentration in the activation stage.

Later in the sequence, $b$-value rises and $Dc$ stabilizes, indicating a redistribution of energy toward smaller, less organized ruptures, consistent with the decay phase of seismic swarm dynamics. The $a_b$ and $q$ values reinforce this interpretation, showing strong deviation from linear scaling, especially during the early phase.

Such behavior supports a hybrid mechanism for seismic swarm generation involving both fault-controlled and triggered by subsurface fluid movement components. This aligns with other documented seismic swarms in volcanic and hydrothermal systems, such as those observed in Kolumbo and Vogtland.

## 6. Conclusion

These findings may assist in short-term forecasting of potential volcanic unrest, given that decreasing b-values and increasing Dc often precede eruptive behavior in other volcanic swarms (McNutt, 2025).

The 2025 Santorini-Amorgos seismic swarm represents a textbook example of a hybrid seismic process governed by both tectonic faulting and fluid migration. The dynamic interplay of decreasing b-values and increasing Dc during the seismic swarm activation phase underscores a fractal cascade of rupture development from small to larger scales. This is reversed in the decay phase, reflecting a dissipation of energy into smaller ruptures.

The evolution of the αb and q-parameters provides further evidence of the complexity in rupture scaling and the influence of fluid-rock interactions. The upward migration of seismicity from depth suggests that fluids may have played a triggering role, especially early in the sequence.

Fractal and scaling analysis of such seismic swarms not only elucidates the physics of rupture but also offers practical insight for short-term hazard assessment in regions of combined tectonic and volcanic activity.

## References

Abe, S. and Suzuki, N. (2003): Law for the distance between successive earthquakes, *J. Geophys. Res. – Solid Earth*, **108**, B2, https://doi.org/10.1029/2002JB002220.

Aki, K. (1965): Maximum likelihood estimate of $b$ in the formula $\log N = a - b\,M$ and its confidence limits, *B. Earthq. Res. I. Tokyo*, **43**, 237–239.

Ambraseys, N. (2009): *Earthquakes in the Mediterranean and Middle East: A multidisciplinary study of seismicity up to 1900*. Cambridge University Press, 945 pp.

Andinisari, R., Konstantinou, K. I. and Ranjan, P. (2021): Seismicity along the Santorini–Amorgos zone and its relationship with active tectonics and fluid distribution, *Phys. Earth Planet. In.*, **312**, 106660, https://doi.org/10.1016/j.pepi.2021.106660.

Arriaga, M. C. S., Tsompanakis, Y. and Samaniego, F. (2008): Geothermal manifestations and earthquakes in the caldera of Santorini, Greece: A historical perspective, in: *33rd Workshop on Geothermal Reservoir Engineering: Proceedings*. Stanford University, Stanford, available at https://pangea.stanford.edu/ERE/pdf/IGAstandard/SGW/2008/suarez.pdf.

Bohnhoff, M., Rische, M., Meier, T., Becker, D., Stavrakakis, G., & Harjes, H. P. (2006). Microseismic activity in the Hellenic Volcanic Arc, Greece, with emphasis on the seismotectonic setting of the Santorini–Amorgos zone, *Tectonophysics*, **423**(1–4), 17–33.

Grassberger, P. and Procaccia, I. (1983): Measuring the strangeness of strange attractors, *Physica D: Nonlinear phenomena*, **9**(1–2), 189–208, https://doi.org/10.1016/0167-2789(83)90298-1.

Gutenberg, B. and Richter, C. F. (1944): Frequency of earthquakes in California, *Bull. Seismol. Soc. Am.*, **34**(4), 185–188, https://doi.org/10.1785/BSSA0340040185.

Keranen, K. M., and Weingarten, M. (2018). Induced seismicity, *Ann. Rev. Earth Planet. Sci.*, **46**(1), 149–174.

Mandelbrot, B. (2002). *Gaussian self-affinity and fractals: globality, the earth, 1/f noise, and R/S*. Springer Science & Business Media.

McNutt, S. (2025): Long swarms and short swarms at volcanoes: Evidence for different processes, *Ann. Geophys.*, **68**(1), V109, https://doi.org/10.4401/ag-9156.

Mitchell, T. M. and Faulkner, D. R. (2008): Experimental measurements of permeability evolution during triaxial compression of initially intact crystalline rocks and implications for fluid flow in fault zones, *J. Geophys. Res. - Solid Earth,* **113**(B11), B11412, https://doi.org/10.1029/2008JB005588.

Mogi, K. (1963): Experimental study on the mechanism of the earthquake occurrences of volcanic origin, *B. Volcanol.* **26**, 197–208, https://doi.org/10.1007/BF02597286.

Nomikou, P., Carey, S., Papanikolaou, D., Croff Bell, K., Sakellariou, D., Alexandri, M. and Bejelou, K. (2012): Submarine volcanoes of the Kolumbo volcanic zone NE of Santorini Caldera, Greece, *Global. Planet. Change*, **90–91**, 135–151, https://doi.org/10.1016/j.gloplacha.2012.01.001.

Okal, E. A., Synolakis, C. E., Uslu, B., Kalligeris, N. and Voukouvalas, E. (2009): The 1956 earthquake and tsunami in Amorgos, Greece, *Geophys. J. Int.,* **178**(3), 1533–1554, https://doi.org/10.1111/j.1365-246X.2009.04237.x.

Papazachos, B. C. and Papazachou, C. B. (1997): *The earthquakes of Greece*. Ziti Publications, Thessaloniki, 304 pp.

Scholz, C. H. (2019): *The mechanics of earthquakes and faulting*. Cambridge University Press, 519 pp, https://doi.org/10.1017/9781316681473.

Telesca, L. (2010): Nonextensive analysis of seismic sequences, *Physica A*: *Statistical Mechanics and its Applications*, **389**(9), 1911–1914, https://doi.org/10.1016/j.physa.2010.01.012.

Warren, N. W., and Latham, G. V. (1970). An experimental study of thermally induced microfracturing and its relation to volcanic seismicity, *J. Geophys. Res.*, **75**(23), 4455–4464.

Wiemer, S. and Wyss, M. (2000): Minimum magnitude of completeness in earthquake catalogs: Examples from Alaska, the Western United States, and Japan, *Bull. Seismol. Soc. Am.*, **90**(4), 859–869, https://doi.org/10.1785/0119990114.

Wyss, M. (1973): Towards a physical understanding of the earthquake frequency distribution, *Geophys. J. R. Astron. Soc*, **31**(4), 341–359, https://doi.org/10.1111/j.1365-246X.1973.tb06506.x.

Utsu, T. (1965): A method for determining the value of $b$ in a formula log $N = a - b\,M$ showing the magnitude–frequency relation for earthquakes, *Geophys. Bull. Hokkaido University*, **13**, 99–103, https://doi.org/10.14943/gbhu.13.99.

SAŽETAK

## Karakteristike seizmičkog roja Santorini-Amorgos 2025

*Emil Oynakov, Irena Aleksandrova i Mariya Popova*

Ova studija istražuje prostorno-vremensku evoluciju i karakteristike skaliranja seizmičkog roja iz 2025. godine u regiji Santorini–Amorgos, jednoj od seizmički i vulkanski najaktivnijih zona u Egejskom luku. Koristeći katalog potresa visoke rezolucije, koji obuhvata 1601 događaj ($M_L \geq 2{,}9$), analiziramo varijacije u ključnim statističkim parametrima – uključujući $b$-vrijednost, fraktalnu dimenziju ($Dc$), ekspo-nent skaliranja ($ab$) i $q$-parametar – unutar kumulativnih vremenskih prozora. Naši nalazi otkrivaju izraženo smanjenje b-vrijednosti i istovremeno povećanje Dc tokom faze aktivacije roja, što je u skladu s inverznom energetskom kaskadom i progresivnim prekidom. Prostorni opseg seizmičkog roja ($L$) značajno se smanjuje prije širenja tokom faze raspadanja, dok vertikalna migracija seizmičkog baricentra ukazuje na proces nukleacije potaknut fluida. Trodimenzionalne vizualizacije potvrđuju klasterizaciju usklađenu s rasjedima, kao i obrasce vertikalne migracije, što podržava hibridni mehanizam rupture kojim upravljaju i tektonski rasjedi i difuzija fluida.

Ovi rezultati pružaju ključan uvid u složenu dinamiku seizmičkih rojeva u ekstenzionim vulkanskim okruženjima i naglašavaju značaj fraktalne analize i analiza skaliranja za kratkoročnu procjenu seizmičke opasnosti.

*Ključne riječi*: seizmički roj, Santorini-Amorgos, b-vrijednost, fraktalna dimenzija, skaliranje rupture, interakcija fluid-rasjed, migracija potresa

*Corresponding author's address*: Irena Aleksandrova, National Institute of Geophysics, Geodesy and Geography, Bulgarian Academy of Sciences, Acad. G. Bonchev St., bl. 3, 1113 Sofia, Bulgaria; e-mail: i.alex@abv.bg